Supplementary Information

Probing Drug Pharmacokinetics by Neutron Scattering Techniques

Clara B. Martins[a,d], Mona Sarter[b], Ana L. M. Batista de Carvalho[a], Victoria García-Sakai[b], Tilo Seydel[c], Jacques Ollivier[c], Luís A. E. Batista de Carvalho[a] and Maria P. M. Marques*[a,d]

[a]*University of Coimbra, Dep. Chemistry, Molecular Physical-Chemistry - LAQV Requimte, Portugal*
[b]*ISIS Neutron and Muon Source, STFC Rutherford Appleton Laboratory, Chilton, Didcot, OX11 0QX, UK*
[c]*Institut Max von Laue – Paul Langevin (ILL), CS 20156, F-38042 Grenoble, France*
[d]*University of Coimbra, Dep. Life Sciences, Portugal*

Table of Contents

Methods

Synthesis of Pd_2Spm
QENS Fundamentals
QENS Data Analysis

Supplementary Figures

References

Methods

Synthesis of Pd_2Spm

The Pd_2Spm complex was synthesised according to published procedures [1], optimised by the authors [2]: 2 mmol of K_2PdCl_4 were dissolved in a minimal amount of water and 1 mmol of spermine aqueous solution was added dropwise, under continuous stirring. After 24 h, the resulting orange powder was filtered and washed with acetone, and the yellow-orange needle-shaped crystals were recrystallized from water. The newly synthesized compound was characterized (and tested for purity) by ^{1}H-NMR and vibrational spectroscopies (FTIR, Raman and inelastic neutron scattering), the latter being compared with previous experimental and calculated (*ab initio* methods) vibrational profiles [2]. Yield: 68%. Elemental analysis ($Pd_2(C_{10}N_4H_{26})Cl_4$): Found – C: 21.2%; H: 4.7%; N: 9.6%, Cl: 25.9%; Calculated – C: 21.5%; H: 4.6%; N: 9.9%, Cl: 25.6%.

Stock solutions of the drugs – either cisplatin or Pd_2Spm – were freshly prepared by dissolving an appropriate amount of drug in PBS (phosphate buffer saline, H_2PO_4 1.5 mM, Na_2HPO_4 4.3 mM, KCl 2.7 mM, NaCl 150 mM, pH 7.4) containing 10% of DMSO. The solutions were sterile-filtered and stored at -20 °C.

QENS Fundamentals

Quasi-elastic neutron scattering (QENS) analyses the scattering signal resulting from a variety of atomic motions taking place at pico- to nanosecond time scales, ranging from fast vibrational and rotational localised modes to slower diffusional modes. This method is typically used under the assumption that the observed scattering can be treated as incoherent, as it is dominated by the incoherent interaction between hydrogen atoms and neutrons (hydrogen has a much larger incoherent scattering cross section compared to that of other elements). The QENS signal which is a direct measure of the dynamic structure factor, S(Q,ω), arises from all dynamical processes which fall in the spectrometer's time window. It represents energy (ħω) and momentum (Q) exchanges between the neutrons and the atoms within the sample and is observed as a broadening about an elastic line of energy exchange ≈0. The signal measured experimentally can be expressed as:

$$S_{\text{measured}}(Q,\omega) = \exp\left(-\frac{\hbar\omega}{2kT}\right) R(Q,\omega) \otimes S(Q,\omega) \quad (1)$$

where exp(-ħω/2kT) is a detailed balance parameter, and R(Q,ω) is the instrument´s resolution function (experimentally obtained) which is convoluted with the dynamic structure factor (S(Q,ω)) that describes the dynamical behaviour of the sample. In hydrogenous biological compounds, where S(Q,ω) is dominated by the large incoherent scattering from hydrogen atoms, it is typically analysed as a convolution of vibrational, rotational and translational components which are assumed to be independent motions,

$$S_{\text{inc}}(Q,\omega) = S_{vib}(Q,\omega) \otimes S_{rot}(Q,\omega) \otimes S_{trans}(Q,\omega) \quad (2)$$

Strictly in the elastic and quasielastic regions,

$$S_{inc}(Q,\omega) = exp\big(-Q^2\langle u^2\rangle\big)\big[A_0(Q)\delta(\omega) + \big(1 - A_0(Q)\big)L(Q,\omega)\big] \quad (3)$$

where the exponential term is the Debye-Waller factor, $A_0(Q)\delta(\omega)$ is the elastic contribution arising from motions slower than the longest observable time as defined by the energy

resolution of the spectrometer, and the second term in the equation corresponds to the quasielastic component. $S_{inc}(Q,\omega)$ provides time/space information on the system probed, on the time scale of the dynamical processes (through the neutron energy transfer, ω), and on the spatial extent of these processes (from the momentum scattering transfer, Q). Since the QENS data in the time domain is represented by an exponential, it can be approximated in the energy domain by Lorentzian functions of different widths,

$$L(q,\omega) = \frac{1}{\pi} \frac{\Gamma(q)}{\Gamma(q)^2 + \omega^2} \quad (4)$$

Γ being the full width at half-maximum (FWHM=2xHWHM (half-width at half-maximum)). These Lorentzian functions describe motions occurring on different lengthscales, detailed information on each dynamic component being retrieved from the Q-dependency of Γ.

S(Q,w) functions are measured directly on QENS spectrometers such as IN5 and IN16B at the ILL. In addition, an efficient method called fixed window scans (FWS) is available on IN16B, whereby instead of measuring the full range of energy transfers at a fixed temperature the scattering signal is scanned at a fixed energy as a function of temperature. Each scan is taken at a fixed energy transfer point (1, 2, 3, …) of the QENS curve (Fig. S7). Since the scans are obtained in different areas of the QENS profile, this information must be taken into account when interpreting the data [3].

As indicated above, dynamic information is contained in the peak broadening (FWHM). By recording the intensity of the scattered data *vs* Q at different energy transfers, the apparent MSD $< u_{\omega}^2 >$ can be calculated for that specific energy transfer, according to the following equation:

$$\log [S(Q,\omega)] = -\frac{1}{3} \cdot (b + \langle u^2 \rangle_{\omega} \cdot Q^2 + c \cdot Q^4) \quad (5)$$

This allows us to infer the dynamic behaviour of the systems and how it changes under different conditions, in this case temperatures.

Additionally, the intensity integrated over Q in the incoherent range, and its variation with temperature, provides information on the relative flexibility of the samples. For this there are two approaches: (i) the elastic fixed window scan, where a higher intensity at 0 μeV reveals a larger elastic contribution and thus a reduced dynamics within the analysed timescale; (ii) the FWS at 0.9, 1.3, and 2 μeV (in IN16B), which sit on different areas of the broadened QENS peak. Analysing these intensity changes with a variation in temperature allows to determine if the corresponding dynamic change increases or decreases with temperature [3]. In IN5, elastic intensity (EI) measurements were performed as a function of T (100 – 310 K), over 0 energy transfer.

QENS Data Analysis

The quasi-elastic neutron scattering data was binned for better statistics and grouped (into 10 groups for IN5 and 8 groups for IN16B). The data was reduced from raw time-of-flight signals into energy transfer spectra using the MANTID routine (Manipulation and Analysis Toolkit for Instrument Data, version 6.11.0) [4].

QENS spectra were corrected for detector efficiency. Resolution functions were determined independently from calibration runs for: (i) vanadium used for detector efficiency corrections; (ii) drug-protein adducts at low temperature (*ca.* 2 K) used as resolutions for data analysis.

The experimental data was fitted to existing models previously optimised by the authors [5-7], to obtain diffusion coefficients and relaxation times. Fitting of the QENS spectra was performed within the energy transfer range -2 to 2 meV, for a Q-range of 0.3 to 1.2 $Å^{-1}$ for IN5, and -0.31-0.31 meV for a Q-range of 0.43 to 1.21 $Å^{-1}$ for IN16B, to ensure negligible coherent scattering contributions to the signal (the incoherent assumptions hold [8]), using the DAVE software (version 2.5, developed at the National Institute of Standards and Technology (NIST) Center for Neutron Research) [9]. The systems were accurately represented by applying one Dirac Delta function to account for very slow hydrogen motions whose center of mass appears immobile within the instrument resolution (elastic component) and two Lorentzians that describe all mobile atoms within the instrument´s timescale (quasielastic contributions). In addition, an energy independent instrumental background was applied.

FWHM values were extracted from each of the Lorentzian functions, and the translational diffusion coefficients (D_T) and reorientation times (τ_T, the mean residence time of a water molecule in each possible location) (at temperature T) were obtained according to a non-diffusive jump reorientation model [10, 11] that follows the equation:

$$\Gamma_T(Q) = \frac{D_T Q^2}{1 + D_T Q^2 \tau_T} \tag{6}$$

Supplementary Figures

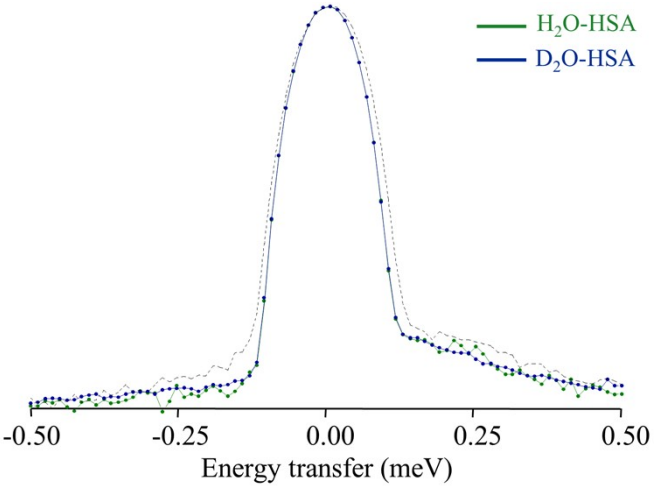

Figure S1. QENS profiles, measured at IN5, at 100 K (Q=1.2036 Å^{-1}, logarithmic scale) for H_2O-hydrated and D_2O-hydrated HSA.
(The spectra are normalised to maximum peak intensity. The dashed line represents the instrument resolution, as measured by a standard vanadium sample).

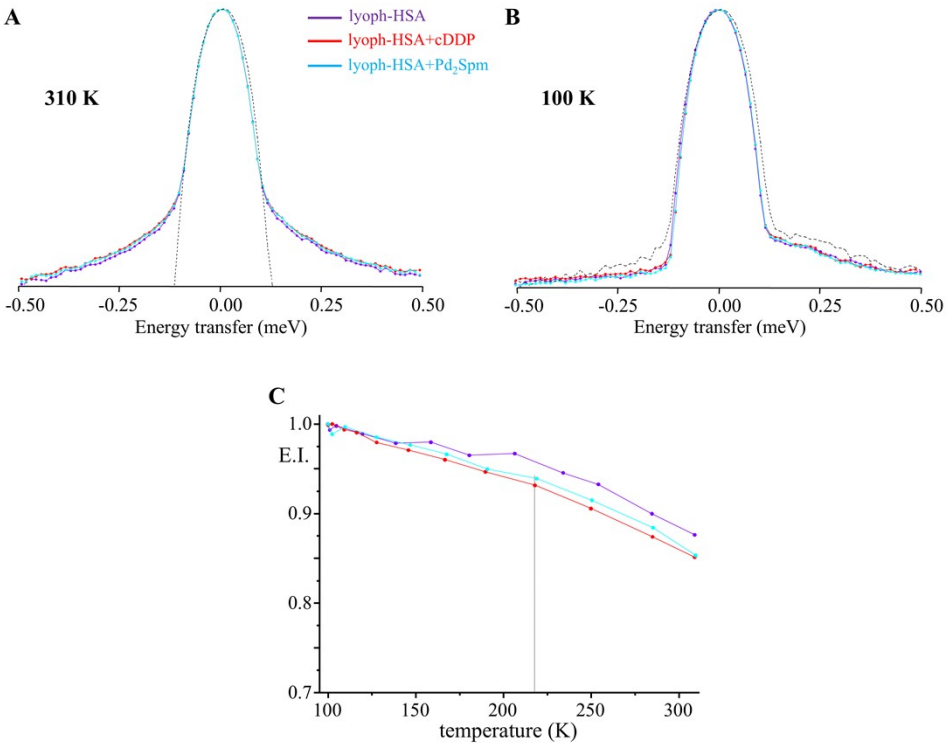

Figure S2. QENS profiles (at 310 and 100 K, Q=1.2036 Å^{-1}, logarithmic scale) (A and B) and plots of elastic intensity (EI) as a function of T (100 – 310 K) (C), measured at IN5 (at 0 μeV), for lyophilised HSA and the corresponding drug-HSA adducts.
(The spectra are normalised to maximum peak intensity. The dashed line represents the instrument resolution, as measured by a standard vanadium sample. The elastic intensity data was obtained over 0 energy transfer).

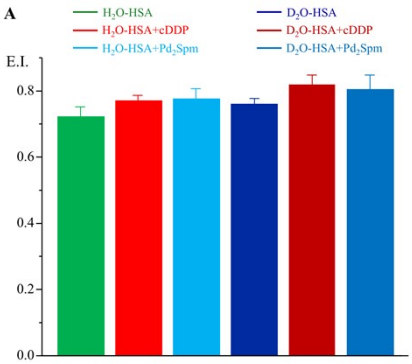

Figure S3. Plots of elastic intensity, at 310 K, measured at IN5, for H_2O-hydrated HSA, D_2O-hydrated HSA and the corresponding drug-HSA adducts.

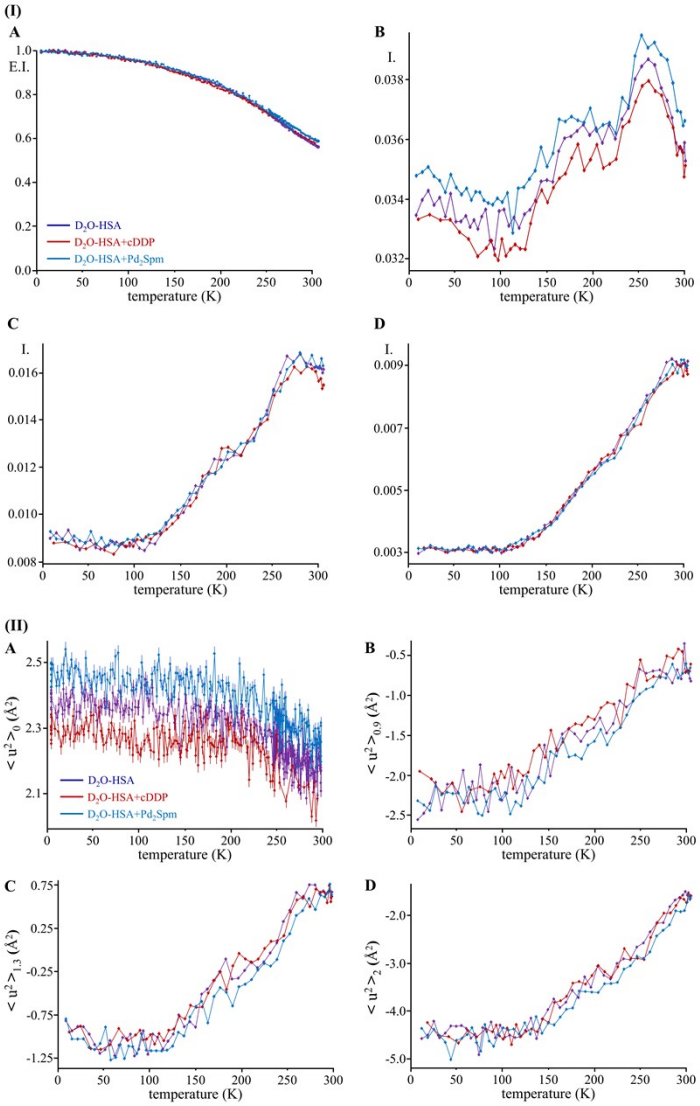

Figure S4 (I). FWS as a function of T (5 – 310 K), obtained at IN16B, for D_2O-HSA, D_2O-HSA+cDDP and D_2O-HSA+Pd_2Spm, at 0 μeV (A), 0.9 μeV (B), 1.3 μeV (C) and 2.0 μeV (D). (Plot (A) represents the normalised elastic intensity integrated over the instrument resolution, while (B) to (D) represent the non-normalised intensity at different energy transfers). **(II)** Temperature variation of the generalized mean-square displacements (5 – 310 K), obtained at IN16B, for D_2O-HSA, D_2O-HSA+cDDP and D_2O-HSA+Pd_2Spm, at 0 μeV (A), 0.9 μeV (B), 1.3 μeV (C) and 2.0 μeV (D).

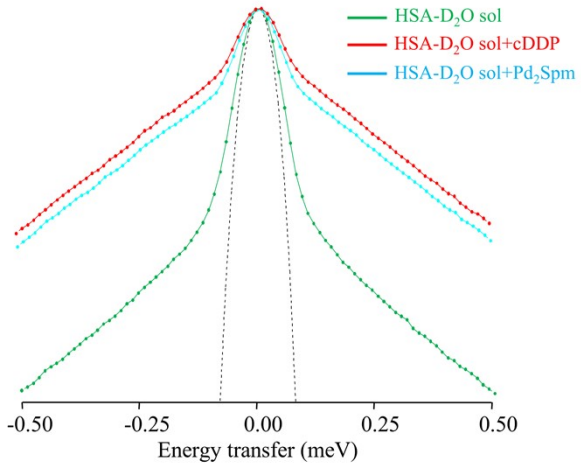

Figure S5. QENS profiles, at 310 K, measured at IN5 (averaged over the entire Q range, logarithmic scale), for HSA and the corresponding drug-HSA adducts in D_2O solution.
(The spectra are normalised to maximum peak intensity. The dashed line represents the instrument resolution, as measured by a standard vanadium sample).

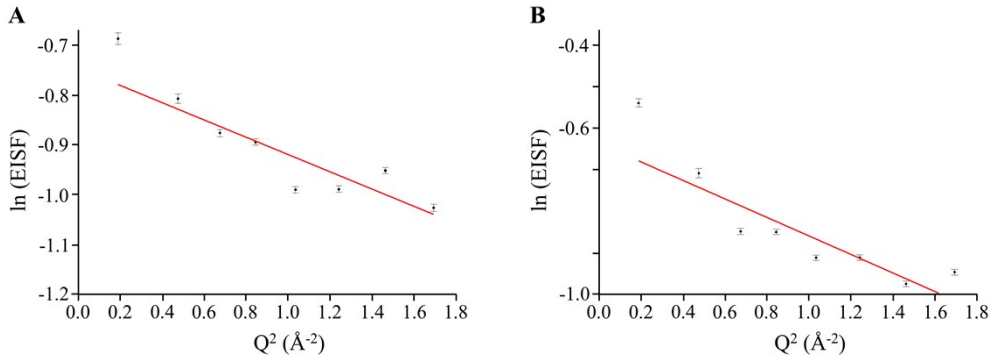

Figure S6. Fits of ln(EISF) *vs* Q^2 to determine the MSD´s (at 310 K) for: (A) D_2O-HSA; (B) D_2O-HSA+Pd_2Spm. (The results are shown in Table 3 of the main manuscript).

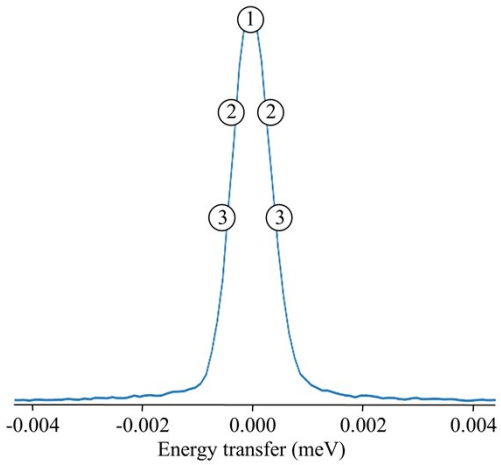

Figure S7. Example of a QENS spectrum illustrating how FWS scans are taken. (More than the 3 indicated energy transfers can be scanned).

References

1. G. Codina, A. Caubet, C. López, V. Moreno and E. Molins, *Helvetica Chimica Acta*, 1999, **82**, 1025-1037.
2. S. M. Fiuza, A. M. Amado, S. F. Parker, M. P. M. Marques and L. A. E. Batista de Carvalho, *New Journal of Chemistry*, 2015, **39**, 6274-6283.
3. C. Beck, F. Roosen-Runge, M. Grimaldo, D. Zeller, J. Peters, F. Schreiber and T. Seydel, *J Appl Crystallogr*, 2024, **57**, 912-924.
4. O. Arnold, J. C. Bilheux, J. M. Borreguero, A. Buts, S. I. Campbell, L. Chapon, M. Doucet, N. Draper, R. Ferraz Leal, M. A. Gigg, V. E. Lynch, A. Markvardsen, D. J. Mikkelson, R. L. Mikkelson, R. Miller, K. Palmen, P. Parker, G. Passos, T. G. Perring, P. F. Peterson, S. Ren, M. A. Reuter, A. T. Savici, J. W. Taylor, R. J. Taylor, R. Tolchenov, W. Zhou and J. Zikovsky, *Nuclear Instruments and Methods in Physics Research Section A: Accelerators, Spectrometers, Detectors and Associated Equipment*, 2014, **764**, 156-166.
5. M. P. Marques, A. L. Batista de Carvalho, V. G. Sakai, L. Hatter and L. A. Batista de Carvalho, *Phys Chem Chem Phys*, 2017, **19**, 2702-2713.
6. M. P. M. Marques, A. L. M. Batista de Carvalho, A. P. Mamede, A. Dopplapudi, S. Rudic, M. Tyagi, V. Garcia Sakai and L. A. E. Batista de Carvalho, *Molecules*, 2020, **25(2)**, 246.
7. M. P. M. Marques, I. P. Santos, A. L. M. Batista de Carvalho, A. P. Mamede, C. B. Martins, P. Figueiredo, M. Sarter, V. G. Sakai and L. A. E. Batista de Carvalho, *Phys Chem Chem Phys*, 2022, **24**, 15406-15415.
8. M. Sarter, J. R. Stewart, G. J. Nilsen, M. Devonport and K. Nemkovski, *J Am Chem Soc*, 2024, **146**, 28023-28033.
9. R. G. Azuah, L. G. Kneller and Y. Qiu, Journal of Research of the National Institute of Standards and Technology, 2009, **114(6)**.
10. D. Laage, *J Phys Chem B*, 2009, **113**, 2684-2687.
11. D. Laage, T. Elsaesser and J. T. Hynes, *Chem Rev*, 2017, **117**, 10694-10725.